Human haptoglobin phenotypes and concentration determination by nanogold-enhanced electrochemical impedance spectroscopy

2011 Nanotechnology 22 245105

(http://iopscience.iop.org/0957-4484/22/24/245105)

Nanotechnology **22** (2011) 245105 (9pp) doi:10.1088/0957-4484/22/24/245105

Human haptoglobin phenotypes and concentration determination by nanogold-enhanced electrochemical impedance spectroscopy

Tsai-Mu Cheng[1,5], Tzu-Cheng Lee[1,5], Shin-Hua Tseng[1,5], Hsueh-Liang Chu[1], Ju-Pin Pan[2,3] and Chia-Ching Chang[1,4,6]

[1] Department of Biological Science and Technology, National Chiao Tung University, Hsinchu 30050, Taiwan, Republic of China
[2] Division of Cardiology, Department of Medicine, Taipei Veterans General Hospital, Taipei 11217, Taiwan, Republic of China
[3] School of Medicine, National Yang-Ming University, Taipei 11217, Taiwan, Republic of China
[4] Institute of Physics, Academia Sinica, Taipei 11529, Taiwan, Republic of China

E-mail: ccchang01@faculty.nctu.edu.tw

Received 1 March 2011, in final form 7 April 2011
Published 4 May 2011
Online at stacks.iop.org/Nano/22/245105

Abstract

Haptoglobin (Hp) is an acute phase protein that binds free hemoglobin (Hb), preventing Hb-induced oxidative damage in the vascular system. There are three phenotypes in human Hp, whose heterogeneous polymorphic structures and varying concentrations in plasma have been attributed to the cause of diseases and outcome of clinical treatments. Different phenotypes of Hp may be composed of the same subunits but different copy numbers, rendering their determination difficult by a single procedure. In this study, we have developed a simple, fast, reliable and sensitive method, using label-free nanogold-modified bioprobes coupled with self-development electrochemical impedance spectroscopy (EIS). By this method, probe surface charge transfer resistance is detected. The relative charge transfer resistance ratios for Hp 1-1, Hp 2-1 and Hp 2-2 were characterized. We were able to determine protein size difference within 3 nm, and the linear region of the calibration curve for Hp levels in the range of 90 pg ml^{-1} and 90 μg ml^{-1} ($\sim$1 fM to 1 pM). We surmise that similar approaches can be used to investigate protein polymorphism and altered protein–protein interaction associated with diseases.

(Some figures in this article are in colour only in the electronic version)

1. Introduction

Haptoglobin (Hp) is an acute phase protein that binds free hemoglobin (Hb) to prevent Hb-induced oxidative damage [1, 2]. Hp is a multi-sub-unit-containing protein, and the $\alpha\beta$ heterodimer is the fundamental structural unit, where α represents an α_1 or α_2 subunit. As illustrated in figure 1, there are three Hp phenotypes in humans: Hp 1-1, Hp 2-1 and Hp 2-2. Hp 1-1 is the simplest combination with dimeric $\alpha_1\beta$ ($[\alpha_1\beta]2$). Type Hp 2-1 is a heterogeneous linear polymer, $\alpha_1\beta$–$(\alpha_2\beta)n$–$\alpha_1\beta$, where n is an integer number from 0 to 2, etc. Type Hp 2-2 is a circular polymer, $(\alpha_2\beta)n$, where n is an integer number from 3, 4, etc [3, 4]. The mean trimer particle sizes for Hp 2-1 and Hp 2-2 are 10.9 and 13.0 nm, respectively. However, the average size of homogeneity Hp 1-1 is 11.6 nm by STEM [5]. Although the size difference among these heterogeneous polymorphic structures of Hp is within 3 nm, they considerably affect the biological functions and thereby

[5] These authors contributed equally.
[6] Address for correspondence: Department of Biological Science and Technology, National Chiao Tung University, Hsinchu 30050, Taiwan, Republic of China.

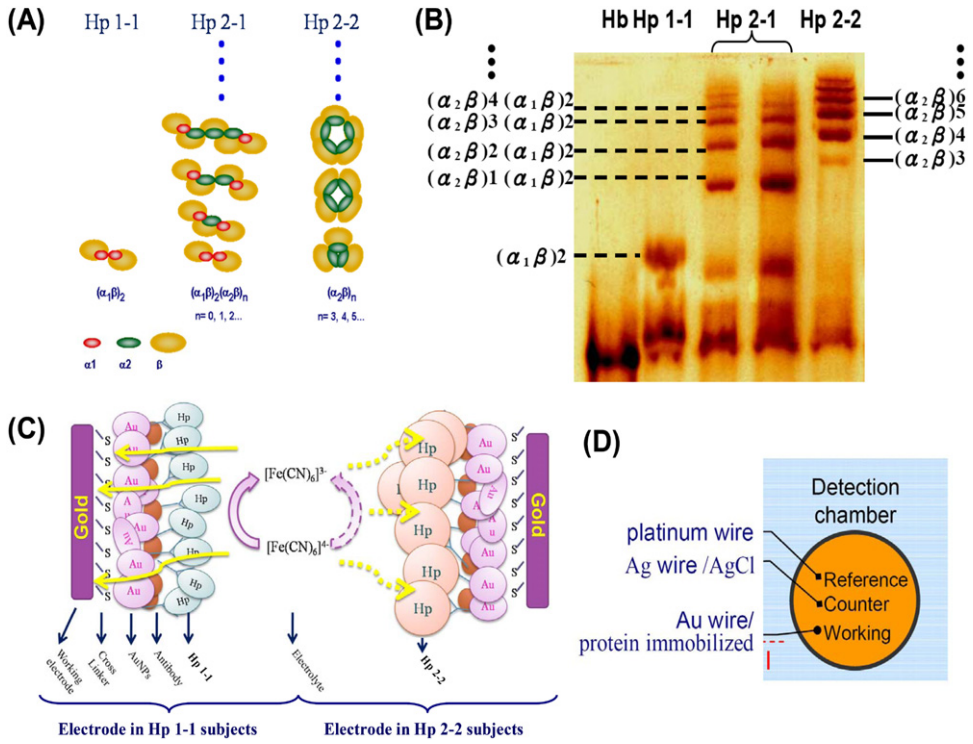

Figure 1. A schematic model illustrating the structure of human Hp phenotypes and the description of the immunosensor on the electrode surface. (A) Hp 1-1 represents a homodimer and is the simplest combination of dimeric $\alpha_1\beta$ chains $(\alpha_1\beta)2$. Hp 2-1 is a linear heterogeneous polymer that is composed of $\alpha_1\beta$–$(\alpha_2\beta)n$–$\alpha_1\beta$, where $n = 0$–3, etc. Hp 2-2 is a cyclic heterogeneous polymer with $(\alpha_2\beta)n$, where $n = 3$–5, etc. (B) Hp phenotyping by electrophoresis of Hb-supplemented plasma followed by DAB staining. (C) A schematic diagram illustrating the reaction between the redox electrode (2.5 mM $[Fe(CN)_6]^{4-/3-}$ in PBS (pH 7.4)) and the electrode surface. Hp 2-2 has larger stereohindrance, resulting in a larger electroresistance than Hp 1-1 on the electrode surface. (D) A schematic model illustrating the structure of the lab-generated three-electrode cell reaction chamber.

have clinical consequences. For example, Hp 1-1 individuals are twice as susceptible to mortality due to coronary heart disease (CHD) and liver diseases compared with those having other Hp phenotypes [4, 6]. Moreover, Hp 1-1 is associated with sickle cell disease, acute and chronic myeloid leukemia, and acute lymphoid leukemia [7]. In contrast, Hp 2-2 individuals are more susceptible to diabetic and cardiovascular diseases than those with other phenotypes [4] and Hp 2-2 patients with coronary artery diseases (CAD) are more likely to develop restenosis after percutaneous tarnsluminal coronary angioplasty [8]. Furthermore, Hp phenotype determination in patients with suspected Kawasaki disease (KD) may facilitate proper treatment by physicians of the disease to prevent cardiac complications [9]. In addition, Hp concentration could be used as an index factor for certain diseases. For example, a low concentration of plasma Hp can be used as an index for the reactive hemophagocytic syndrome in adult-onset Still's disease [10] or hemolytic disease. In contrast, Hp concentration is markedly increased in patients with inflammation [11].

The precise phenotype and plasma concentration determination of Hp is crucial for successful clinical treatments. Hence, real-time and effective methods for routine tasks such as deciding Hp phenotype and plasma level are required during the early stages of a variety of diseases. Conventional laboratory practice for Hp phenotyping relies on labor-intensive electrophoresis, chromogen staining [3, 12] (figure 1(B)) or chemiluminescent imaging [3, 12] and they are time-consuming and expensive for clinical applications.

Antigen–antibody immunochemical sensors have been the subject of intensive investigation over the past few years because their sensitivity would satisfy the selectivity requirement for clinical diagnosis [13, 14]. Immunosensors involve an antigen or antibody immobilized onto a solid-state surface that participates in biospecific antigen–antibody binding, allowing detection and quantification of the reactants of interest. Most immunoassay techniques are similar to ELISA, which is based on a solid phase sandwich immunoassay [3]. Biosensors for Hp phenotyping were not reported until this study. For Hp concentration determination the surface plasmon resonance (SPR) [15] or high-speed spinning-desk interferometry were to be reported [16]. Phenotyping must be performed before Hp quantization because of the structure polymorphism among the Hp types [3]. These methods are not efficient for high-throughput tasks in clinical diagnosis. Therefore, a more efficient immunochemical method for clinical analysis of Hp is required for clinical diagnosis in the early stages of many diseases. We have designed a highly sensitive Bio-Electrochemical Analyzer and sensor probes to determine Hp phenotypes and their plasma concentration by detecting the protein–antibody signals of cyclic voltammetry (CV) and electrochemical impedance spectroscopy (EIS) based on the heterogeneous sizes among Hp types. The EIS technique has been applied in the prostate

cancer cell test [17]. This powerful technique monitors events on the sensing electrodes and has shown promise for point-of-case and real-time monitoring [14, 18]. In this study, the EIS technique was applied to determine Hp phenotype and plasma concentration in samples from healthy volunteers, using the specific anti-human Hp antibody or Hb electrode probes.

2. Experimental methods

2.1. Materials

Cysteamine (BioChemika grade), 25% glutaraldehyde (Grade I) and sodium citrate were purchased from Sigma-Aldrich. Hydrogen tetrachloroaurate (III) trihydrate (ACS, 99.99%) was purchased from Alfa Aesar. Potassium hexacyanoferrate (III) and potassium hexacyanoferrate [19] were of ACS grade and purchased from J T Baker (Mallinckrodt Baker, Inc., Phillipsburg NJ, USA). All chemicals were used as supplied without further purification. Bovine serum albumin (biotechnology grade) was obtained from Amresco. Phosphate buffered saline (PBS) was prepared by mixing 0.05 M KCl with 0.05 M K_2HPO_4/KH_2PO_4. All solutions were prepared using double-distilled water (ddH_2O).

2.2. Preparation of gold nanoparticles

The monodispersed colloidal gold nanoparticles (AuNPs) used in this study have been previously described [20, 21]. Briefly, aqueous solutions of $HAuCl_4$ (4%, w/w) and sodium citrate (1%, w/w) were prepared in ddH_2O. Chloroauric acid solution (0.5 ml) was added to 200 ml of ddH_2O and was brought to a boil for mixing. Subsequently, sodium citrate (3 ml) was slowly added with vigorous mixing and extended by reflux for 30 min. A dark blue suspension first appeared which turned red as monodispersed colloidal AuNPs were formed. The AuNPs prepared by this method had a specified average particle size of 13 nm [20]. After cooling to room temperature, the AuNPs stock solution was stored at 4 °C for further use.

2.3. Modification and antibody immobilization of the gold electrode

Modification of the working electrode and self-assembled monolayer [14] was performed according to a previously described method (figure 1(C)) [22]. Briefly, a gold electrode was polished with various sizes of abrasive papers followed by aluminum powders (0.3 and 0.05 μm in diameter, respectively) on microcloth pads. Next, the gold electrode was rinsed in ddH_2O water and ultrasonicated in absolute ethanol for 5 min. Subsequently, the electrode was electrochemically polished in a 0.05 M H_2SO_4 solution through potential scanning at a range of 0 to +1.6 V at a scan rate of 100 mV s^{-1} until a stable cyclic voltammogram (CV) was obtained. Following the electrochemical polish, the gold electrode was rinsed with ddH_2O and immersed in a 20 mM cysteamine aqueous solution for 12 h. After removing the physically adsorbed cysteamine with an abundant amount of ddH_2O, the electrode was modified with a glutaraldehyde solution (12%, v/v) for 1 h, rinsed with ddH_2O and soaked in a 0.02 M cysteamine solution for approximately 12 h and rinsed again with ddH_2O. As the self-assembly monolayer [14] is formed, the electrode was immersed immediately in 500 μl of colloidal gold nanoparticles for 10 h and then covered with a monolayer of AuNPs. The newly modified electrode was covered with a droplet of polyclonal (Sigma) or monoclonal antibody (Ab) (anti-human Hp antibody produced by Cheng *et al* [3]), 5 μl, 0.5 mg ml^{-1} in 1× PBS [3] at 4 °C for approximately 12 h and rinsed with PBS (pH 7.4) to thoroughly remove the excess particles physically adsorbed on its surface. Furthermore, the electrode was immersed in bovine serum albumin (BSA) solution (10 mg ml^{-1}) as a blocking reagent for 30 min to block the nonspecific binding sites of the AuNPs. The electrode was washed again with PBS (pH 7.4) and stored at 4 °C until use.

2.4. Electrochemical measurements

All electrochemical measurements were performed with a three-electrode cell. These electrodes were a modified Au electrode (working electrode), a platinum wire (counter electrode) and an Ag/AgCl wire immersed in 3 M KCl (reference electrode; figure 1(D)). All experiments were performed at room temperature and all potentials in this work were measured with direct relevance to the Ag/AgCl reference electrode. The EIS operates with 10 mV AC sinusoidal amplitude and 0.23 V direct current (DC) potential, which is the standard oxidizing potential of 2.5 mM $Fe(CN)_6^{4-/3-}$ (1:1 in 10 mM PB solution (pH 7.4)) and a frequency ranging from 0.1 to 105 Hz. $Fe(CN)_6^{4-/3-}$ acted as a redox probe in this study. The ZSimpWin V3.20 software from Informer Technologies Inc. (TN, USA) was used for simulation to reveal the related electrical parameters of the working electrode.

2.5. Regeneration of the working electrode

Following electrochemical measurements, the contaminated interface of the modified working electrode was regenerated by washing the electrode probe in PBS–ammonia solution (pH 12) at least three times. Once the interactive protein is removed from the electrode, it can be reused to carry out another cycle of electrochemical measurement. The regenerated electrodes were immersed in PBS and stored at 4 °C until further use.

2.6. Phenotype determination of plasma samples

The phenotypes of plasma samples were determined by Hb-supplemented 7% native polyacrylamide gel electrophoresis (PAGE) and peroxidase chromogen staining to detect Hb peroxidase activity, as described by Cheng *et al* [3], as a reference control for comparison with the data by EIS measurements.

3. Results

3.1. Verification of functionalized electrode with cyclic voltammetry

Each step of the surface-modified Au electrode was verified by CV for the biosensor electrode preparation. As indicated in figure 2, the CV responses of the electrode

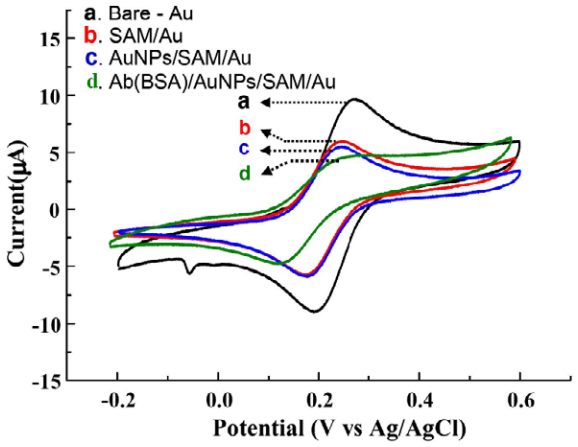

Figure 2. Cyclic voltammetry of the modified electrodes. (a) Bare-Au electrode; (b) SAM/Au-modified electrode; (c) AuNPs/SAM/Au-modified electrode and (d) Ab(BSA)/AuNPs/SAM/Au-modified electrode, formation of immunochemical complex at the surface. The cyclic voltammograms were detected by immersing the electrode in 2.5 mM $[Fe(CN)_6]^{4-/3-}$ in PBS (pH 7.4) at a scan rate of 100 mV s^{-1}.

in various modification stages were measured in 2.5 mM $K_3Fe(CN)_6/K_4Fe(CN)_6$ redox electrolyte in PBS (pH 7.4) with a scan rate of 100 mV s^{-1} between −0.2 and +0.6 V. The CVs of various modification stages of the gold electrode showed that the peak current decreased gradually when the electrode was modified with a self-assembled monolayer (SAM), nanogold, and antibody and antigens, sequentially. In the bare-Au electrode state, a reversible CV with a peak-to-peak separation (ΔI_p) of 16.92 nA was observed (figure 2, curve a). When the bare-Au electrode was modified with cysteamine, glutaraldehyde and cysteamine layers, the amperometric response of the SAM/Au redox electrode decreased to 12.24 nA (figure 2, curve b). Furthermore, when the nanogold was chemically bound to the SAM/Au electrode (denoted as AuNPs/SAM/Au), the amperometric response decreased further ($\Delta I_p = 11.59$ nA) (figure 2, curve c). When the nanogold-linking electrode was linked with anti-human Hp Ab followed by blocking the non-conjugated nanogold with BSA (Ab(BSA)/AuNPs/SAM/Au), the final CV response current (ΔI_p) decreased to 7.53 nA (ΔI_p) (figure 2, curve d), which was attributed to the binding of Ab and BSA on the surface of the nanogold.

3.2. Plasma Hp phenotype determination by impedance measurement

During each stage of electrode modification, CV spectra were measured to confirm the successful linkage of added molecules to the electrode surface. EIS measurement was accomplished by immersing the functionalized electrodes in 50 μl of different Hp phenotype plasma samples for 5 min, and the Hp phenotype of each sample was examined from the Nyquist plot. The EIS response of the electrode immersed in Hp-free plasma was used as the baseline control. Detailed data regression analysis with a Randles model showed no significant change in the R_{ct} of baseline controls. Meanwhile, the plasma samples showed

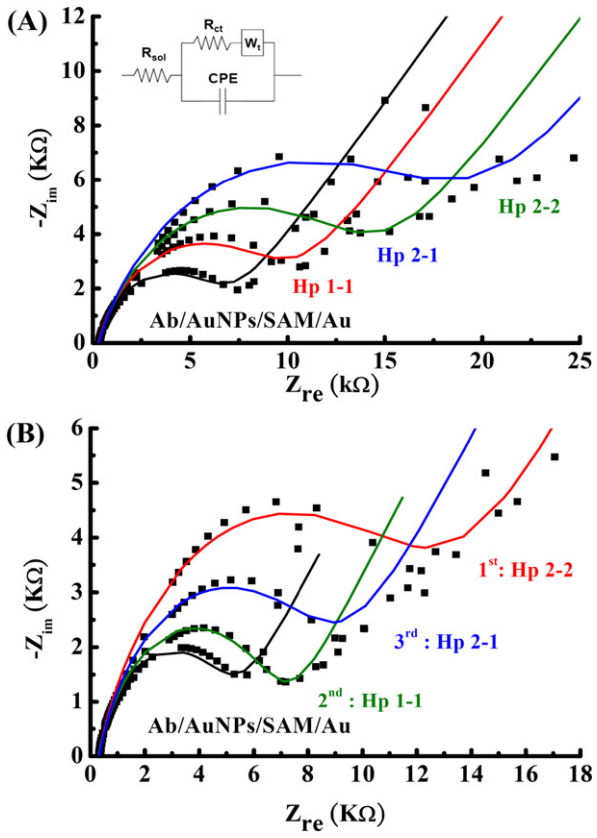

Figure 3. Nyquist plot of EIS measurement of different Hp phenotypes on an Au electrode immobilized with Hp-specific antibody. The impedance behavior of the electrolyte can be fitted to a Randles model (A, inset) that includes the solution resistance (R_{sol}), charge transfer resistance (R_{ct}), constant phase element (CPE) and Warburg impedance element (W_t). (A) Detection of different Hp phenotypes of human plasma; once the Hp molecule is captured on the device, the graph shows a clear increase in impedance with the sequence: baseline → Hp 1-1 → Hp 2-1 → Hp 2-2. (B) Reusability of an Hp–Ab-immobilized electrode and its reproducible Hp detection. The graph shows repeating measurement results after each electrode recovery with the detection sequence: baseline → Hp 2-2 → Hp 1-1 → Hp 2-1 → baseline.

an increasing R_{ct} trend in the series measurement of Hp 1-1, Hp 2-1 and Hp 2-2 (figure 3(A)). Our data suggest that the increase of R_{ct} was due to stereohindrance produced by structural polymorphisms among various Hp phenotypes (figure 1(A)). The Hp 2-2 subtype has the largest amount of polymorphic structures and the largest packing density on the electrode surface. Therefore, it resulted in the greatest change of charge transfer resistance (R_{ct}) on the electrode. In contrast, Hp 1-1 has the smallest homogeneous structure among other Hp species and resulted in the smallest R_{ct} change on the electrode (figure 1(C)). Hp 2-1 exhibited a midrange R_{ct} between Hp 1-1 and Hp 2-2. Similar trends of purified Hp measurement were observed in the Nyquist plot (data not shown). The trend of semicircle diameters was Hp 2-2 > Hp 2-1 > Hp1-1 > baseline.

3.3. Stability and reusability of the Hp phenotyping electrode for EIS measurement

The resuming test order was baseline → Hp 2-2 → Hp 1-1 → Hp 2-1 → baseline. As indicated in figure 3(B), the

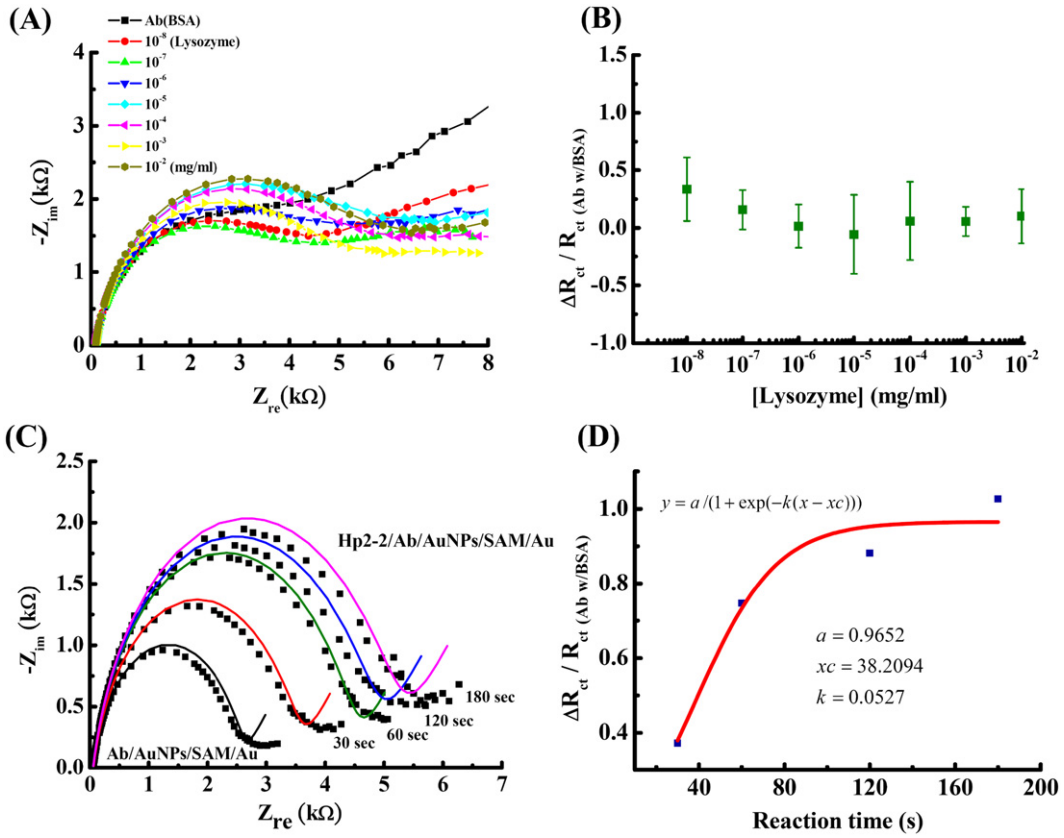

Figure 4. Influence of nonspecific binding and incubation time of antibody and antigen. (A) EIS results with various lysozyme concentrations; a small difference was observed among the semicircle from 0 to 10 μg ml^{-1}. (B) Relative charge transfer resistance ratio ($\Delta R_{ct}/R_{ct}$) of various concentrations of lysozyme. (C) The electrode was immersed in the same clinical sample at various interactive times. The EIS results closely overlap at incubation times longer than 120 s. (D) The relative charge transfer resistance ratio ($\Delta R_{ct}/R_{ct}$) of various Hp 2-2 incubation times.

regenerated electrodes can replicate the Hp phenotype data, which is similar to figure 3(A). Namely, the electrode can be easily regenerated for future applications to determine the Hp phenotype and this regeneration method possesses high repeatability of the EIS response. The relative charge transfer resistance ratios ($\Delta/R_{ct(Abw/BSA)}$), described in section 3.4, of all electrodes to distinguish the various reactants in Hp phenotype determination showed relative standard deviation (RSD) mean values of 8.79%, 4.12% and 6.5% for Hp 2-2, Hp 2-1 and Hp 1-1, respectively. This process revealed that the active Ab on the electrode surface could be regenerated in appropriate conditions.

3.4. Binding specificity assay of the Hp phenotyping electrode

To confirm the binding specificity of Hp phenotyping electrodes, a positively charged lysozyme was tested with the Hp–Ab-immobilized electrode. The Nyquist plot in figure 4(A) shows that the EIS response of the electrode to lysozyme was similar to the baseline control. Slight changes were observed during the measurement as the concentration of lysozyme was varied. The data plotted as $\Delta R_{ct}/R_{ct(Abw/BSA)}$ reflect the relative increase of charge transfer resistance compared to $R_{ct(Abw/BSA)}$, where $R_{ct(Abw/BSA)}$ represents the baseline of charge transfer resistance when the Ab-immobilized electrode was immersed in Hp-free plasma. The ΔR_{ct} corresponded to the change of charge transfer resistance of plasma sample detection relative to $R_{ct(Abw/BSA)}$. The data show that there was no significant change in the transfer resistance among the detections of various lysozyme concentrations (figure 4(B)).

3.5. Optimization of incubation times between Ab-immobilized electrode and Hp 2-2 samples

The Nyquist plot of different incubation times between the Ab-immobilized electrode and Hp 2-2 samples is shown in figure 4(C). The semicircle diameter of the Nyquist plot increased when the incubation time was increased, indicating that the incubation time affects the detection outcome and that the signal reached a steady state after 120 s incubation. The change was small at incubation times longer than 120 s (figure 4(D)). The Nyquist plot indicated that most of the Ab immobilized on the electrode reacted with the Hp molecules in the plasma sample. According to the results in figures 4(C) and (D), 2 min of incubation would be sufficient for Hp phenotype determination for practical use.

3.6. Correlation between Hp phenotypes and relative R_{ct} change for plasma samples

Figure 5 shows the relative charge transfer resistance ratio of various Hp phenotypes. The result reflects the polymorphic

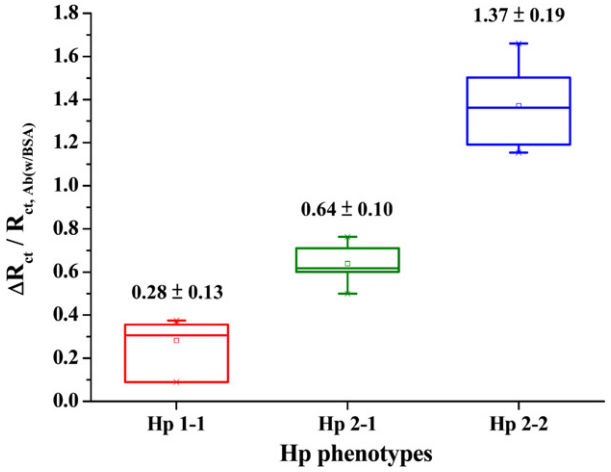

Figure 5. Prediction of Hp phenotype by relative charge transfer resistance ratio ($\Delta R_{ct}/R_{ct(Abw/BSA)}$). The ($\Delta R_{ct}/R_{ct(Abw/BSA)}$) corresponds to the relative transfer resistance change of various phenotypes of clinical samples detected on the Hp–Ab-immobilized electrode. The ($\Delta R_{ct}/R_{ct(Abw/BSA)}$) was calculated by complex nonlinear least-squares regression of EIS measurement with Randles model. Hp 2-2 had the largest relative change transfer resistance change compared with baseline (1.37 ± 0.19), Hp 1-1 had the smallest (0.28 ± 0.13) and Hp 2-1 was in the midrange (0.64 ± 0.10).

structural polymerization of various Hp phenotypes [3]. The detected plasma sample sizes were 4, 12 and 12 for Hp 1-1 (0.28 ± 0.13), Hp 2-1 (0.64 ± 0.10) and Hp 2-2 (1.37 ± 0.19), respectively. Therefore, we estimated that the relative charge transfer resistance ratio value is higher than 0.90 for the Hp 2-2 type, lower than 0.45 for the Hp 1-1 type and within 0.5–0.75 for the Hp 2-1 type.

3.7. Application of plasma Hp concentration determination by EIS compared to conventional ELISA assay

This study used the designed Au/SAM/AuNPs/Ab electrode for Hp detection to determine plasma Hp concentrations. The diameter of the semicircle of Nyquist plots decreased when the concentration of Hp 2-2 was diluted from 90 μg ml^{-1} to 90 pg ml^{-1} (figure 6(A)). These results reflected the decreased binding of Hp to the Ab-immobilized electrode, which in turn decreased the relative charge transfer resistance ratio. Therefore, the concentration of Hp can be determined using this approach. The different slopes of serially diluted (from 60 μg ml^{-1} to 60 pg ml^{-1}) Hp 2-2 and Hp 1-1 can be distinguished using calibration with the relative charge transfer resistance ratio (figure 6(B)). This difference may be attributed to the structural polymorphisms among Hp phenotypes that result in different charge resistance ratio slopes.

3.8. The Hb-based EIS measurement

Figure 6(C) shows that Hb-based EIS can successfully identify Hp phenotypes in Nyquist plots. Similar to the Ab-immobilized electrode, Hb binding with Hp 2-2 resulted in the largest packing density on the electrode surface and resulted in

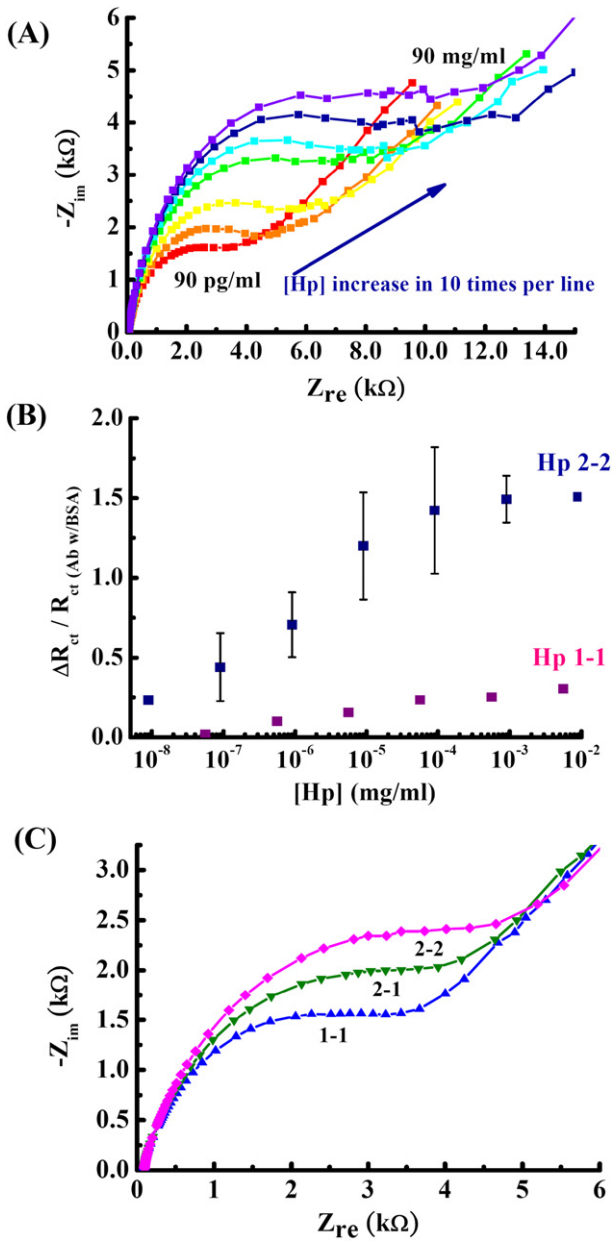

Figure 6. Dose response of Hp immunosensor and phenotypes on hemoglobin-immobilized electrodes. (A) Nyquist plots of various concentrations of Hp 2-2 (90 pg ml^{-1} to 90 μg ml^{-1}) in clinical samples. The sample was diluted ten times from 90 μg ml^{-1} to 90 pg ml^{-1}. (B) The relative charge transfer resistance ratio of various Hp concentration values showing linear calibration curves of Hp 2-2 and Hp 1-1. (C) Once Hp molecules were captured by Hb on the electrode, the Nyquist plot of EIS showed a clear increase in the semicircle diameter that was related to the charge transfer resistance with the sequence: baseline → Hp 1-1 → Hp 2-1 → Hp 2-2.

the greatest change of charge transfer resistance (R_{ct}) on the electrode.

Hp 1-1 has the smallest structure, resulting in the smallest change of R_{ct} on the electrode. Hp 2-1 showed an R_{ct} between Hp 1-1 and Hp 2-2. Similar trends of Nyquist plot were detected in the Hb-immobilized electrode (figure 6(C)). The same semicircle diameter trend was

observed with the Ab-immobilized electrode: Hp 2-2 > Hp 2-1 > Hp 1-1 > baseline.

4. Discussion

The charge transfer through the barrier or the defect in the barriers between the solution species and the electrodes follows the tunneling effect [23] and the CV can be used to monitor the modification condition of the sensing electrode during the functionalization process. Moreover, the nanogold-modified layer reduces the steric hindrance of protein SAM formation and increases the coverage density on the electrode. In addition, the nanogold layer reduces the resistance between the electrode and solution. Therefore, the CV current of this modified electrode may be generally higher than the conventional electrode and the CV changes in various modification stages can be identified clearly (figure 2). This CV response of the nanogold-modified electrode is better than previously reported [23]. Moreover, the nanogold-modified electrode in the EIS system may reduce the effective impedance and increase the detection sensitivity in general. Therefore, the detection limit can be pushed to 90 pg ml^{-1} (approximately in the sub-fM range) of Hp (figure 6), which is more sensitive than the conventional detection process. The detailed mechanism will be discussed below.

The peak of CV current decreased from curve a to curve d in figure 2, which could be attributed to the gradual increase in packing density on the electrode. Namely, the electron transfer between the redox electrolyte (2.5 mM $[Fe(CN)_6]^{4-/3-}$ in pH 7.4) in solution and the electrode surface was gradually blocked by the sequential modification process of the electrode. Therefore, we may infer that the modification of the working electrode can be monitored by CV measurement.

EIS is an effective and label-free method to probe the interfacial properties of a modified electrode and to characterize immunocomplexes [22, 24]. In this study, an anti-Hp immobilized electrode was investigated to determinate Hp phenotype. The impedance response of a functionalized electrode that is immersed in electrolyte with a redox probe (2.5 mM $[Fe(CN)_6]^{4-/3-}$ in pH 7.4) can be described by the Randles model (figure 3(A), inset). In the Randles model, R_{sol} is the resistance of the electrolyte and R_{ct} is the charge transfer resistance of the redox probe on the surface of the working electrode. W_t denotes the Warburg impedance, which is contributed by the diffusion process of the redox probe and is related to the low-frequency part of the impedance spectroscopy, and CPE is the constant phase element, which is the electric double-layer capacitance and reflects the heterogeneity of the surface layer in the presence of immobilized protein molecules. Therefore, R_{ct} and CPE reflect the dielectric and insulating features at the electrode/electrolyte interface that are controlled by the surface modification of the electrode [19, 25]. A Nyquist plot of EIS was used to record the impedance data of Hp phenotyping (figures 3, 4, 6(A) and (C)). The impedance, Z, was expressed in terms of its real (Zre) and negative imaginary ($-Z$im) components. In the plot, there existed a semicircle in the low impedance region with diameter equal to R_{ct} according to the Randles model. Therefore, the Nyquist plot is a convenient way to reveal the change of R_{ct}. When the working electrode binds to particular biomolecules, the EIS of the Nyquist plot is a powerful tool to qualitatively identify the existence of the interaction of biomolecules on the electrode surface by measuring the change of charge transfer resistance, R_{ct}. Since there are only four components and five parameters that are contained in the Randles model, at least five different scanning frequencies are sufficient to obtain these parameters. Moreover, an impedance test at stimulus frequencies greater than 1 Hz can be completed within a few seconds. For rapid detection and better electrical parameter determination from the Randles model, a comprehensive range of scanning frequencies can be modified into a few points with wide distribution and the entire EIS measuring time can be completed within 2 or 3 min.

Regeneration capability is a key factor in the development of a practical immunosensor. Immunosensor regeneration is achieved by removing bound Hp from the Ab-immobilized electrode by immersing the electrode in PBS–ammonia (pH 12). The regenerated probe can be used for the EIS assays of another plasma sample, and all Hp phenotypes of a plasma sample are therefore determined using the same regenerated probe. The regenerated working electrodes were stored in PBS (pH 7.4). After several detection → regeneration cycles (within two months), a decrease was observed in R_{ct} in the Nyquist plot but not in $\Delta R_{ct}/R_{ct(Abw/BSA)}$, implying good electrode stability in our regeneration and storage process.

The specific binding property is one of the most important factors in immunoassay. In general, the major contribution of nonspecific binding is caused by electrostatic interactions between the negatively charged Ab-immobilized electrode and other counter ion molecules [25]. According to the EIS measurement results, the Hp–Ab-immobilized electrode presents specific binding to Hp.

The Nyquist plots of EIS are not convenient for routine clinical judgment because of the nonhomogeneity of the probes. However, one of the electrical parameters, the relative change of $R_{ct}(\Delta R_{ct}/R_{ct})$ that was derived from measuring data, was distinguishable for different Hp phenotypes and could be used directly for on-site detection. Because the relative charge transfer resistance ratios change caused by the different haptoglobin polymorphic particle sizes, Hp 2-1 trimer and Hp 2-2 trimer are 10.9 and 13.0 nm, respectively. In addition, the homogeneity Hp 1-1 is 11.6 nm [5]. It denote that the present EIS method can distinguish the particle size difference within 1–3 nm by charge transfer resistance change. The relative charge transfer resistance ratio ($\Delta R_{ct}/R_{ct(Abw/BSA)}$) has been used to distinguish the various reactants in immunosensors [26]. According to the measurement results shown in figure 5, we have developed a biosensor that is convenient, time saving and easy to handle for on-site Hp phenotype determination.

According to figure 6(B), the sensitivity of the EIS measurement reaches the pg ml^{-1} level, which is higher than the conventional measurement of μg ml^{-1} –ng ml^{-1} as measured by ELISA [3]. Our EIS method is also more sensitive than the reported biosensor, BioCD [16], which can detect at

the ng ml^{-1} level. In addition to sensitivity, the EIS sensor can detect the phenotype before protein determination, which is important for the determination of Hp concentrations using their own calibration curve [3]. According to the EIS result, the Hp concentration determination by the Hp typing calibration curve [3] is more sensitive using EIS than the traditional ELISA method.

In spite of the receptor-ligand-based biosensors [14, 27], we tested the application of EIS on protein–protein interactions. Hp is an Hb binding protein that avidly binds to red blood cell (RBC)-free Hb with a binding affinity of approximately $>10^{10}$ M [1, 2]. Hb is relatively easy to purify using general laboratory techniques [28] and is therefore used instead of anti-Hp antibody for EIS measurement. The results shown in figure 6(C) indicate that an appropriate protein immobilized on the electrode surface can be used as a probe to reveal protein–protein interactions. Therefore, our electrode can be successfully applied to plasma Hp phenotyping and plasma concentration determination and, in addition, is a potential tool for protein–protein interaction studies.

Many diseases are associated with a single-protein structural polymorphism, and EIS measurement might therefore have potential on-site applications. For example, Huntington's disease (HD), an autosomal dominant disorder, is associated with more than 36 CAG (encoding for polyglutamine) repeats in the HD gene (HTT) [29]. Parkinson's disease, another autosomal dominant disorder, is caused by genomic multiplications of the alpha-synuclein gene (SNCA). The phenotype of SNCA multiple copy number is clinically associated with the severity of the disease [30]. The androgen receptor (AR) gene contains a CAG repeat that is extremely polymorphic in length and the polymorphism influences the functional activity of AR. Several epidemiologic studies showed that polymorphisms of the CAG repeat are associated with an increased risk of prostate cancer [31, 32] and other steroid hormone-related tumors, such as breast [33], endometrial [34] and ovarian [35] cancer. In addition, beta-amyloid protein aggregation is related to the pathogenic mechanism in Alzheimer's disease [36, 37]. All diseases mentioned above are associated with a single-protein polymorphism that results in heterogeneity in protein molecular weight.

5. Conclusions

We confirmed that protein polymorphisms can be identified by the charge transfer resistance ratio of the protein-bound electrode from the measurement of EIS. In this study, we propose that a simple detection method based on the measurement of relative charge transfer resistance ratio by EIS is a potential approach for investigating the polymorphism by changes in molecular weight. We believe that this procedure can be applied in the future to screen the protein polymorphisms that are related to the clinical diagnosis of diseases.

Acknowledgments

We would like to thank Dr P C Huang in Johns Hopkins University, Dr T N Baral in the National Research Council Canada, Institute of Biological Sciences (NRC-IBS) and Dr M Sundaram in the Department of Biochemistry, Microbiology, and Immunology, University of Ottawa for their valuable suggestions on this paper. This project was supported in part by an NSC grant (97-2112-M-009-009-YM3) and the ATU-MOE Project, Taiwan, ROC.

References

[1] Kristiansen M, Graversen J, Jacobsen C, Sonne O, Hoffman H, Law S and Moestrup S 2001 Identification of the haemoglobin scavenger receptor *Nature* **409** 198
[2] Schaer C, Vallelian F, Imhof A, Schoedon G and Schaer D 2007 CD163-expressing monocytes constitute an endotoxin-sensitive Hb clearance compartment within the vascular system *J. Leukoc. Biol.* **82** 106
[3] Cheng T, Pan J, Lai S, Kao L, Lin H and Mao S 2007 Immunochemical property of human haptoglobin phenotypes: determination of plasma haptoglobin using type-matched standards *Clin. Biochem.* **40** 1045
[4] Kymberley C and Mark W 2007 Haptoglobin: a review of the major allele frequencies worldwide and their association with diseases *Int. J. Lab. Hematol.* **29** 92
[5] Wejman J C, Hovsepian D, Wall J S, Hainfeld J F and Greer J 1984 Structure and assembly of haptoglobin polymers by electron microscopy *J. Mol. Biol.* **174** 343
[6] De Bacquer D, De Backer G, Langlois M, Delanghe J, Kesteloot H and Kornitzer M 2001 Haptoglobin polymorphism as a risk factor for coronary heart disease mortality *Atherosclerosis* **157** 161
[7] Langlois M R and Delanghe J R 1996 Biological and clinical significance of haptoglobin polymorphism in humans *Clin. Chem.* **42** 1589
[8] Ariel R, Irit H, Eugenia N, Walter M, Simcha R M, Jamal H, Ehud G, Rafael B and Andrew P L 2001 Haptoglobin phenotype as a predictor of restenosis after percutaneous transluminal coronary angioplasty *Am. J. Cardiol.* **87** 330
[9] Lee W, Hwang K, King Y, Chen H, Chiou S, Yang R and Huang T 2000 Late diagnosis of Kawasaki disease is associated with haptoglobin phenotype *Eur. J. Clin. Invest.* **30** 379
[10] Hot A, Toh M-L, Coppere B, Perard L, Girard Madoux M H, Mausservey C, Desmurs-Clavel H, Ffrench M and Ninet J 2010 Reactive hemophagocytic syndrome in adult-onset still disease: clinical features and long-term outcome: a case-control study of 8 patients *Medicine* **89** 37
[11] Komozi G F, Samann M D, Buchta C, Peck-Radosavljevic M, Mayr W R, Schwartz D W M, Dunkler D, Spitzauer S and Panzer S 2006 Influence of clinical factors on the haemolysis marker haptoglobin *Eur. J. Clin. Invest.* **36** 202
[12] Huang G, Ouyang J, Delanghe J R, Baeyens W R G and Dai Z 2004 Chemiluminescent image detection of haptoglobin phenotyping after polyacrylamide gel electrophoresis *Anal. Chem.* **76** 2997
[13] Daniels J and Pourmand N 2007 Label-free impedance biosensors: opportunities and challenges *Electroanalysis* **19** 1239
[14] Hou Y *et al* 2007 A novel detection strategy for odorant molecules based on controlled bioengineering of rat olfactory receptor I7 *Biosens. Bioelectron.* **22** 1550
[15] Choi S and Chae J 2009 A microfluidic biosensor based on competitive protein adsorption for thyroglobulin detection *Biosens. Bioelectron.* **25** 118
[16] Nolte D D 2009 High-speed spinning-disk interferometry on the biocd for human diagnostic applications *Conf. Proc. IEEE Eng. Med. Biol. Soc.* p 6368
[17] Yun Y, Dong Z, Shanov V N and Schulz M J 2007 Electrochemical impedance measurement of prostate cancer

cells using carbon nanotube array electrodes in a microfluidic channel *Nanotechnology* **18** 465505
[18] Yanga G J, Huangb J L, Menga W J, Shena M and Jiao X A 2009 A reusable capacitive immunosensor for detection of Salmonella spp. based on grafted ethylene diamine and self-assembled gold nanoparticle monolayers *Anal. Chim. Acta* **647** 159
[19] Huang Y, Bell M and Suni I 2008 Impedance biosensor for peanut protein ara h 1 *Anal. Chem.* **80** 9157
[20] Grabar K C, Freeman R G, Hommer M B and Natan M J 1995 Preparation and characterization of Au colloid monolayers *Anal. Chem.* **67** 735
[21] Schneider G and Decher G 2008 Functional core/shell nanoparticles via layer-by-layer assembly. Investigation of the experimental parameters for controlling particle aggregation and for enhancing dispersion stability *Langmuir* **24** 1778
[22] He Y, Luo H and Li N 2007 Thermodynamic and kinetic analysis of the interaction between hepatitis B surface antibody and antigen on a gold electrode modified with cysteamine and colloidal gold via electrochemistry *Biosens. Bioelectron.* **22** 2952
[23] Tang D-P, Yuan R and Chai Y-Q 2006 Novel immunoassay for carcinoembryonic antigen based on protein A-conjugated immunosensor chip by surface plasmon resonance and cyclic voltammetry *Bioprocess Biosyst. Eng.* **28** 315
[24] Park J-Y, Lee Y-S, Kim B H and Park S-M 2008 Label-free detection of antibody–antigen interactions on (R)-lipo-diaza-18-crown-6 self-assembled monolayer modified gold electrodes *Anal. Chem.* **80** 4986
[25] Tang H, Chen J, Nie L, Kuang Y and Yao S 2007 A label-free electrochemical immunoassay for carcinoembryonic antigen (CEA) based on gold nanoparticles (AuNPs) and nonconductive polymer film *Biosens. Bioelectron.* **22** 1061
[26] Oliveira M D L, Correia M T S and Diniz F B 2009 Concanavalin A and polyvinyl butyral use as a potential dengue electrochemical biosensor *Biosens. Bioelectron.* **25** 728
[27] Alfinito E, Pennetta C and Reggiani L 2010 Olfactory receptor-based smell nanobiosensors: an overview of theoretical and experimental results *Sensors Actuators* B **146** 554
[28] Liau C, Chang T, Pan J, Chen W and Mao S 2003 Purification of human plasma haptoglobin by hemoglobin-affinity column chromatography *J. Chromatogr.* B **790** 209
[29] Warby S C, Montpetit A, Hayden A R, Carroll J B, Butland S L, Visscher H, Collins J A, Semaka A, Hudson T J and Hayden M R 2009 CAG expansion in the huntington disease gene is associated with a specific and targetable predisposing haplogroup *Am. J. Hum. Genet.* **84** 351
[30] Ibanez P *et al* 2009 α-Synuclein gene rearrangements in dominantly inherited parkinsonism: frequency, phenotype, and mechanisms *Arch. Neurol.* **66** 102
[31] Giovannucci E, Stampfer M, Krithivas K, Brown M, Brufsky A, Talcott J, Hennekens C and Kantoff P 1997 The CAG repeat within the androgen receptor gene and its relationship to prostate cancer *Proc. Natl Acad. Sci.* **94** 3320
[32] Rodriuez-Gonzalez G, Cabrera S, Ramirez-Moreno R, Bilbal C, Diaz-Chico J, Serra L, Chesa N, Cabrera J and Diaz-Chico B 2009 Short alleles of both GGN and CAG repeats at the exon-1 of the androgen receptor gene are associated to increased PSA staining and a higher Gleason score in human prostatic cancer *J. Steroid Biochem. Mol. Biol.* **113** 85
[33] Yu H, Bharaj B, Vassilikos E J K, Giai M and Diamandis E P 2000 Shorter CAG repeat length in the androgen receptor gene is associated with more aggressive forms of breast cancer *Breast Cancer Res. Treat.* **59** 153
[34] Rodriuez G *et al* 2006 Alleles with short CAG and GGN repeats in the androgen receptor gene are associated with benign endometrial cancer *Int. J. Cancer* **118** 1420
[35] Levine D and Boyd J 2001 The androgen receptor and genetic susceptibility to ovarian cancer: results from a case series *Cancer Res.* **61** 908
[36] Luo Y, Smith J, Paramasivam V, Burdick A, Curry K, Buford J, Khan I, Netzer W, Xu H and Butko P 2002 Inhibition of amyloid-beta aggregation and caspase-3 activation by the Ginkgo biloba extract EGb761 *Proc. Natl Acad. Sci. USA* **99** 12197
[37] Meyer-Luehmann M *et al* 2006 Exogenous induction of cerebral β-amyloidogenesis is governed by agent and host *Science* **313** 1781